PERGAMON

International Journal of Heat and Mass Transfer 45 (2002) 47–55

International Journal of HEAT and MASS TRANSFER

www.elsevier.com/locate/ijhmt

Energy separation in shear layers

B. Han [a], R.J. Goldstein [a,*], H.G. Choi [b]

[a] Department of Mechanical Engineering, University of Minnesota-Twin Cities, 125, Mechanical Engineering Building, 111 Church Street S.E., Minneapolis, MN 55455, USA

[b] Department of Aerospace Engineering and Mechanics, University of Minnesota-Twin Cities, Minneapolis, MN 55455, USA

Received 8 August 2000; received in revised form 3 April 2001

Abstract

A numerical analysis is performed to study the mechanism of energy separation in a viscous heat-conducting shear layer. Two-dimensional time-dependent Navier–Stokes equations and total energy conservation equation are solved simultaneously for four different Reynolds numbers: 100, 200, 500, and 1000. The results show that the roll-up and transport of vortices induce pressure fluctuations in the shear layer. Fluid which flows through the disturbed pressure field exchanges pressure work with the surroundings and separates into higher and lower total temperature regions. Even though some energy separation is caused by the imbalance between shear work and heat conduction, that due to the pressure fluctuation is much stronger. As the Reynolds number is increased, turbulence mixing between higher and lower total temperature regions tends to lessen the energy separation. However, the more rapid growth of pressure fluctuations overcomes the weakening of energy separation by random mixing. © 2001 Published by Elsevier Science Ltd.

1. Introduction

Spontaneous separation of the total temperature in different portions of a flowing fluid is called "energy separation". Energy separation presents the possibility to heat or cool fluid without using a conventional heating or cooling system, but rather with a simple flow device (e.g., a Ranque–Hilsch tube). However, current obtainable temperature differences between hot and cold regions for the flow devices are not large enough for some engineering applications. Further research to enlarge the temperature difference is still required. Not only this possibility, but also understanding the mechanism of the phenomena involved is important to predict the accurate temperature distribution in fluid flows where flows are used as heat transfer enhancement methods such as impinging jets.

Since Eckert and Weise [1] first found energy separation from the recovery temperature distribution on a circular cylinder, others have reported the existence of the phenomenon in various flows including boundary layers [2], jet flows [3], cross-flow across a circular cylinder [4], and shear layer [5]. Eckert [6] suggested two physical mechanisms of energy separation. One is the imbalance between the energy transport by viscous shear work and that by heat conduction. The other is due to pressure fluctuation within flow fields caused by moving vortices. Unlike the energy separation by the shear/conduction imbalance, that from pressure fluctuation has time-dependent characteristics. He also pointed out that energy separation of a viscous flow is caused by both mechanisms. Though most previous studies were based on time-averaged temperature measurements, research on the instantaneous mechanism of energy separation is essential to understand the phenomena.

Recently a few studies were performed to investigate the instantaneous mechanism experimentally and numerically. Experiments to measure instantaneous total temperature were performed in the wake of a circular cylinder [7], and a turbine blade [8]. Fox et al. [9] carried out a numerical analysis of the energy separation in a free jet with inviscid and non-conducting fluid assumption. Han and Goldstein [10] performed a numerical analysis of that in a plane shear layer by solving the two-

* Corresponding author. Tel.: +1-612-625-5552; fax: +1-612-625-3434.

E-mail address: rjg@me.umn.edu (R.J. Goldstein).

0017-9310/02/$ - see front matter © 2001 Published by Elsevier Science Ltd.
PII: S0017-9310(01)00131-4

Nomenclature

n	nth time step
c_p	specific heat at constant pressure
p	static pressure which is normalized by $\rho\Delta U^2$
Pr	Prandtl number
Re_{δ_0}	Reynolds number, $Re_{\delta_0} = (\Delta U\delta_0)/v$
S	energy separation factor, $S = (T_t - T_{t,o})/(\Delta U^2/2c_p)$
S'	non-dimensional total temperature fluctuation, $S' = T_t'/(\Delta U^2/2c_p)$
S_{max}, S_{min}	maximum and minimum energy separation factor at given streamwise locations
t	time which is normalized by $\delta_0/\Delta U$
T_t	total temperature
T_t'	total temperature fluctuation
$T_{t,o}$	total temperature of the fluid at the inlet
u', v'	disturbances at the inlet
U_1, U_2	free stream velocities
u_i	velocity component in ith direction which is normalized by Δ_U
u_j^*	disturbance distribution for frequency ω_j
x_1, x	streamwise coordinate which is normalized by δ_0
x_2, y	spanwise coordinate which is normalized by δ_0
Greek symbols	
δ_0	initial shear layer thickness
Δt	time increment
ΔU	velocity difference, $\Delta U = U_2 - U_1$
ϵ	magnitude of disturbance
v	kinematic viscosity of fluid
ω_j	frequency of disturbance
ω_z	vorticity, $\omega_z = (dv/dx) - (du/dy)$
ϕ_j	phase angle of disturbance
θ	non-dimensional total temperature, $\theta = (T_t - T_{t,o})/(\Delta U^2/c_p)$

dimensional Navier–Stokes equations. However, their analysis assumed a non-conducting fluid.

In the present study, a two-dimensional plane shear layer is analyzed numerically to investigate the mechanisms of energy separation. Numerical computations are carried out on instantaneous velocity, pressure, and temperature of a viscous and heat conducting shear layer. Not only the energy separation by the pressure fluctuation, but also that by the shear/conduction imbalance is studied. The effect of Re_{δ_0} on the coherent vortical structure and the energy separation in the shear layer is also investigated. The results reveal the instantaneous mechanism of energy separation and its interaction with other mechanism.

2. Mathematical and numerical formulation

The calculation domain and coordinate system for the two-dimensional flow system are illustrated in Fig. 1. Two fluid streams with different velocity (U_1, U_2) are initially separated by a splitter plate. After merging of the two streams, a shear layer is formed and grows as the flow goes downstream.

The governing equations are mass conservation and unsteady Navier–Stokes equations, and total energy conservation equations. With the assumptions of incompressible and constant properties fluid, two-dimensional mass conservation and Navier–Stokes equations are reduced as follows:

$$\frac{\partial u_i}{\partial x_i} = 0, \tag{1}$$

$$\frac{\partial u_i}{\partial t} + u_j\frac{\partial u_i}{\partial x_j} = -\frac{\partial p}{\partial x_i} + \frac{1}{Re_{\delta_0}}\frac{\partial}{\partial x_j}\left(\frac{\partial u_i}{\partial x_j} + \frac{\partial u_j}{\partial x_i}\right). \tag{2}$$

Since the following are valid in the computational domain

$$u \gg v \quad \text{and} \quad \frac{\partial}{\partial y} \gg \frac{\partial}{\partial x}, \tag{3}$$

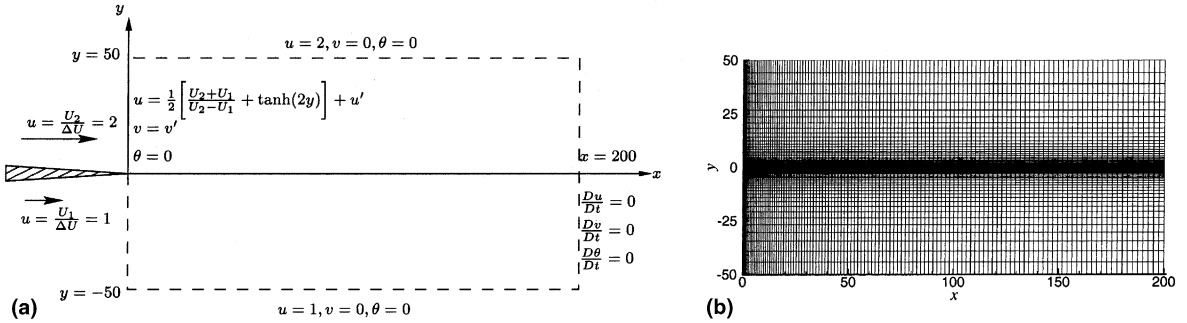

Fig. 1. Schematic diagram of calculation domain, boundary conditions and grids: (a) calculation domain; (b) computational grid.

the "boundary layer approximation" [11] can be applied to total energy conservation equation and it can be written as

$$\frac{\partial\theta}{\partial t}+u_j\frac{\partial\theta}{\partial x_j}=\frac{\partial p}{\partial t}+\frac{1}{Re_{\delta_0}Pr}\frac{\partial}{\partial x_j}\left(\frac{\partial\theta}{\partial x_j}\right)+\frac{1}{Re_{\delta_0}}\left[1-\frac{1}{Pr}\right]\frac{\partial}{\partial y}\left(u\frac{\partial u}{\partial y}\right). \quad (4)$$

When the Prandtl number is close to unity, the last term of Eq. (4) can be neglected and the total energy conservation equation is reduced as follows:

$$\frac{\partial\theta}{\partial t}+u_j\frac{\partial\theta}{\partial x_j}=\frac{\partial p}{\partial t}+\frac{1}{Re_{\delta_0}Pr}\frac{\partial}{\partial x_j}\left(\frac{\partial\theta}{\partial x_j}\right). \quad (5)$$

A numerical algorithm using equal-order linear finite element and fractional four-step method is adopted. Eqs. (1) and (2) are discretized by a procedure similar to that of Choi et al. [12]. Semi-discretized formulation of Eq. (5) with respect to time can be written as follows:

$$\frac{\theta^{n+1}-\theta^n}{\Delta t}+\frac{1}{2}\left[\left(u_j\frac{\partial\theta}{\partial x_j}\right)^{n+1}+\left(u_j\frac{\partial\theta}{\partial x_j}\right)^{n}\right]=\frac{1}{2\Delta t}(p^{n+1}-p^{n-1})+\frac{1}{2Re_{\delta_0}Pr}\left[\frac{\partial}{\partial x_j}\left(\frac{\partial\theta}{\partial x_j}\right)^{n+1}+\frac{\partial}{\partial x_j}\left(\frac{\partial\theta}{\partial x_j}\right)^{n}\right]. \quad (6)$$

Eq. (6) is integrated across the calculation domain to obtain the "weak form" of the total energy conservation equation. The weak form is discretized in space using the equal-order linear finite element method. The set of arithmetic equations obtained by discretization is solved simultaneously with discretized mass conservation and Navier–Stokes equations.

The boundary conditions of the calculation domain are depicted in Fig. 1(a). At the inlet plane ($x=0$), a hyperbolic tangent velocity profile with a very thin initial shear layer is employed. In an actual shear layer, the velocity profile immediately downstream of the splitter plate is wake-like due to the existence of the plate. However, the velocity profile is quickly changed to a hyperbolic tangent-like shape, because of intensive momentum diffusion caused by the large velocity gradient in the spanwise direction. Consequently, the hyperbolic tangent profile assumption is reasonable. To simulate experimental flow conditions, small disturbances are introduced at the inlet plane. The disturbances are obtained from stability analysis of inviscid flow with the same inlet velocity profiles similar to Sandham and Reynolds [13]. The most unstable frequency and its two sub-harmonic frequencies are selected as the frequencies of the disturbance. The magnitude of each disturbance is adjusted so that the turbulence intensity at the inlet plane is less than 1% of ΔU. The boundary condition of u is written in Eq. (7):

$$u(0,y,t)=\frac{1}{2}\left[\frac{U_2+U_1}{U_2-U_1}+\tanh(2y)\right]+\epsilon\sum_{j=1}^{3}u_j^*(y,t)\mathrm{e}^{-\mathrm{i}(\omega_j t+\phi_j)}. \quad (7)$$

Similar disturbances are also introduced in the spanwise velocity component. A uniform total temperature ($T_{\mathrm{t,o}}$) is assumed along the inlet. At the outlet plane, a convective boundary condition is employed to handle vortex passing across the plane [14]. Boundary conditions at the other two boundaries are assumed to be the same as the free stream.

A grid of 120 in x and 75 in y is used with $U_1/\Delta U=1$ and $U_2/\Delta U=2$ (Fig. 1(b)). Calculations are performed with four different Re_{δ_0}: 100, 200, 500, and 1000. Pr is assumed to be 0.7. The velocity, pressure and temperature values are collected after all the initial fields are washed away.

3. Results and discussion

Instantaneous flow and total temperature fields for $Re_{\delta_0}=100$ at different times are shown in Fig. 2. To describe the motion of vortices in the flow, vorticity (ω_z) is used. In the vorticity distribution, a large coherent structure of vortices is observed. This structure is one of typical characteristics in a shear layer. The disturbance applied at the inlet plane starts growing and rolls up into vortices. These small vortices merge with neighboring ones. The merged vortex moves downstream, and combines with another merged one. This interaction was observed in many experimental studies [15,16].

Instantaneous pressure and temperature distributions are presented in Fig. 3. The vortices distort the pressure fields. Pressures near the center of vortices are lower than the surroundings, and there is a local minimum. Between the minimum points, local maximum pressure points exist. These maximum points results from local stagnation of upward and downward flows which occur between two adjacent vortices. Instantaneous total temperature distributions indicate the separation of fluid in higher and lower total temperature regions. The locations of the separation nearly match with those of vortex center. The temperature distribution is asymmetric, which is different from the results of an inviscid calculation [9].

With the observation above, the mechanism of instantaneous energy separation can be explained as follows. Since the vortex is moving with a certain velocity, the distortion in pressure field is also moving. Due to the

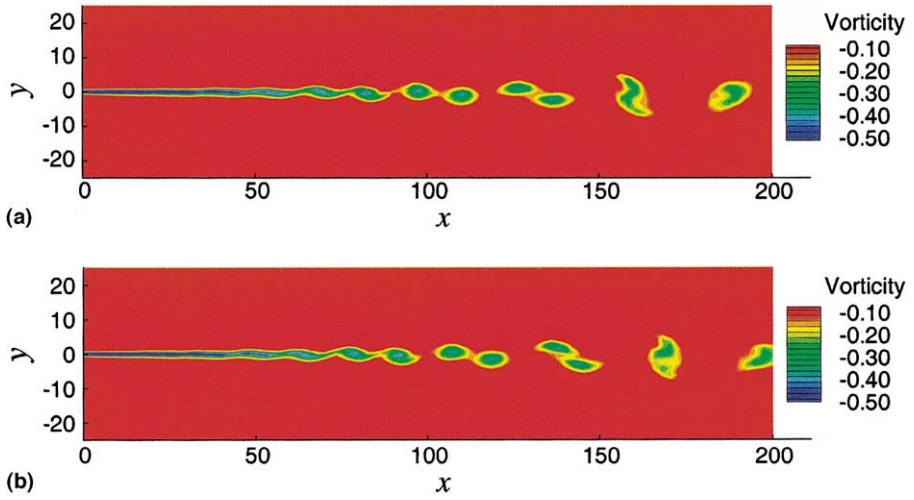

Fig. 2. Instantaneous vorticity distribution for $Re_{\delta_0} = 100$: (a) $t = 250$; (b) $t = 275$.

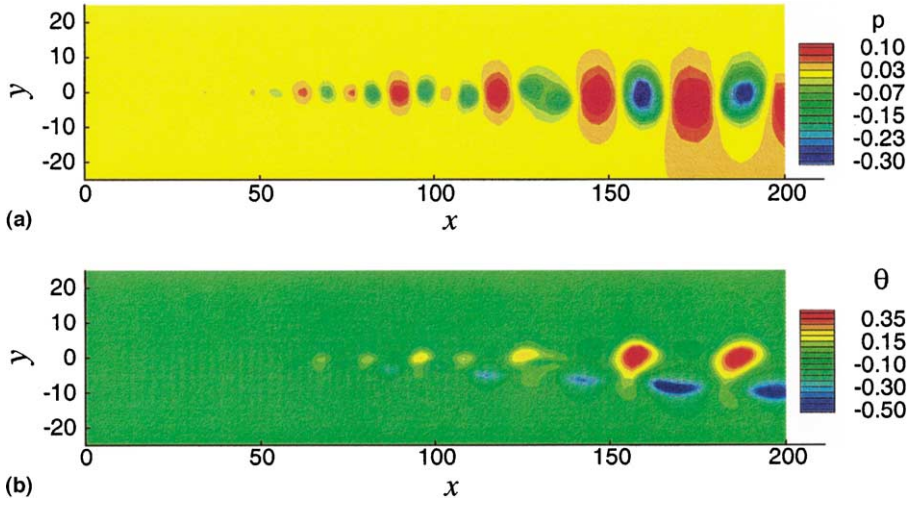

Fig. 3. Instantaneous vorticity distribution for $Re_{\delta_0} = 100$ and $t = 250$: (a) pressure; (b) total temperature.

motion, fluid at the front-half of the vortex experiences negative $\partial p/\partial t$ (i.e., does pressure work on the surrounding fluid), and fluid at the rear-half has a positive $\partial p/\partial t$ (i.e., pressure work done on it by the surrounding fluid is added). Therefore, the fluid loses energy passing through the front-half of the vortex, and gains energy through the rear-half.

In Fig. 4, the pressure around vortices and total temperature variations of fluid packets are illustrated. The thickness of the line represents the pressure at that point, and color denotes the total temperature of the fluid. A fluid packet which enters the flow field from $y > 0$ is entrained into the shear layer through the front-half of the vortices. Along this path, the fluid packet loses energy and reaches its local minimum temperature after passing through $y = 0$. After that, the packet moves upward by the motion of vortex through the rear-half. Along this path, the packet gains energy and returns to nearly its initial total temperature.

Even though a fluid packet from $y < 0$ is entrained similarly, the different sequence of entrainment causes reverse total temperature distribution. Initially the fluid is entrained through the rear-half of the vortex. Due to the entrainment through this path, the packet gains energy first, and reaches a local maximum temperature. These local maximum and minimum total temperatures are indicative of the energy separation.

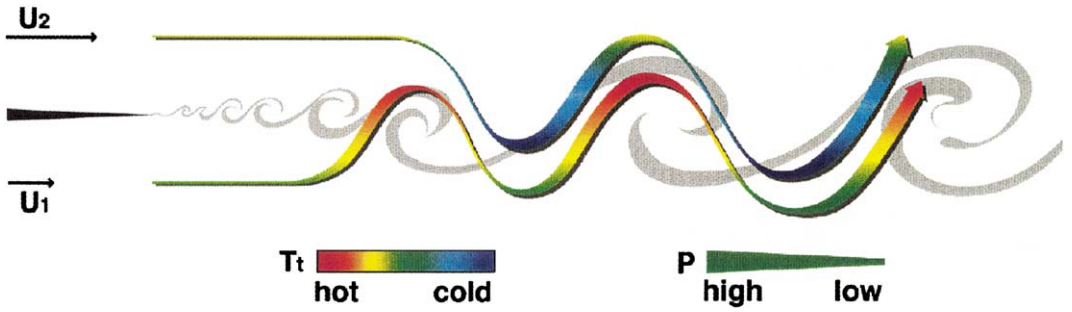

Fig. 4. Schematic diagram of pressure and total temperature variation along pathlines in a shear layer; color denotes the total temperature, and thickness denotes the pressure.

Instantaneous flow and temperature fields with different Re_{δ_0} are shown in Fig. 5. When Re_{δ_0} is larger than 500, small-scale vortices are randomly distributed around large-scale vortices. This implies that increased Re_{δ_0} causes early transition to a turbulent flow. Additionally as Re_{δ_0} increases, the location of the initial vortex roll-up moves upstream. This is caused by more rapid growth of the disturbance due to decreased relative viscous forces. The earlier vortex roll-up due to increased Re_{δ_0} means the earlier initiation of energy separation. Random motion induced by turbulence at high Re_{δ_0} tends to lessen the energy separation by mixing between hot and cold fluids. However, the rapid growth of the disturbance at high Re_{δ_0} results in much more intense pressure fluctuation. As a result, the energy separation is not diminished by random mixing at the highest Re_{δ_0} studied.

Fig. 6 contains time-averaged streamwise velocity profiles at several locations. At $x = 25$, the shear layer thickness for $Re_{\delta_0} = 100$ is slightly thicker than others. This might be due to the development of shear layer up to this region coming mainly from viscous diffusion. However, this trend is reversed as flow goes downstream. At $x = 75$, the development of a shear layer for $Re_{\delta_0} = 500$ and 1000 is noticeable. This can be explained by the vortex motion. Since the growth of the shear layer by vortex motion is more effective than that by viscous diffusion [17], the growth of shear layer at high Re_{δ_0} is faster after the roll-up of vortices.

Fig. 7 shows corresponding energy separation factor profiles. To visualize the total temperature variation, the energy separation factor (S) is used. Unlike the velocity profile, the energy separation factor of $Re_{\delta_0} = 1000$ shows the largest energy separation even at $x = 25$. Energy separation for the other Re_{δ_0} should be mainly due to the imbalance between shear work and heat conduction, since the pressure fluctuation due to the vortex motion is initiated before this location only for $Re_{\delta_0} = 1000$ in the cases studied. This shows that energy separation by the pressure fluctuation is generally much stronger than that by the imbalance of shear work and heat conduction. In Fig. 7(b), the separation for $Re_{\delta_0} = 500$ has increased noticeably, and is close to that of $Re_{\delta_0} = 1000$. It should be noticed that the vortex roll-up is initiated around $x = 50$ in the shear layer when $Re_{\delta_0} = 500$. As the flow goes downstream, this trend is much more apparent. At $x = 100$, the total temperature distributions of $Re_{\delta_0} = 200$, 500, and 1000 are almost similar. This implies that the energy separation is mainly dependent on the pressure fluctuation induced by the vortex motion after a coherent vortical structure is developed.

Fig. 8 shows the total temperature fluctuation (S') at several streamwise locations. The fluctuation of total temperature is almost the same order of magnitude of energy separation amount in time-averaged total temperature distribution. The fluctuations for $Re_{\delta_0} = 500$ and 1000 show two local maxima in Fig. 8(a). Vortices are already initiated for those two cases at $x = 50$. However, the fluctuations for Re_{δ_0} 100 and 200 have only one maximum point. This is thought due to the difference of the major energy separation mechanism. Since the separations for $Re_{\delta_0} = 500$ and 1000 are due to the pressure fluctuation, maximum fluctuation points are expected at upper and lower half-circle [10]. However, the maximum fluctuation point is located at the center of the shear layer, if the energy separation is caused by the imbalance mechanism. At $x = 75$, the fluctuation for $Re_{\delta_0} = 200$ tends to be close to those for $Re_{\delta_0} = 500$ and 1000. However, the fluctuation for $Re_{\delta_0} = 100$ still has only one maximum point.

The variation of maximum and minimum energy separation factors along the streamwise direction is plotted in Fig. 9. This figure shows more clearly the effect of vortex roll-up on energy separation. The rates of change in $S_{\max}$ and $S_{\min}$ increase drastically where the initiation of a vortex is observed. The results verify the explanation that the mechanism of energy separation due to the pressure fluctuation in the transport of vortex motion is much stronger than that from the imbalance of shear work and heat conduction. Note that the rate

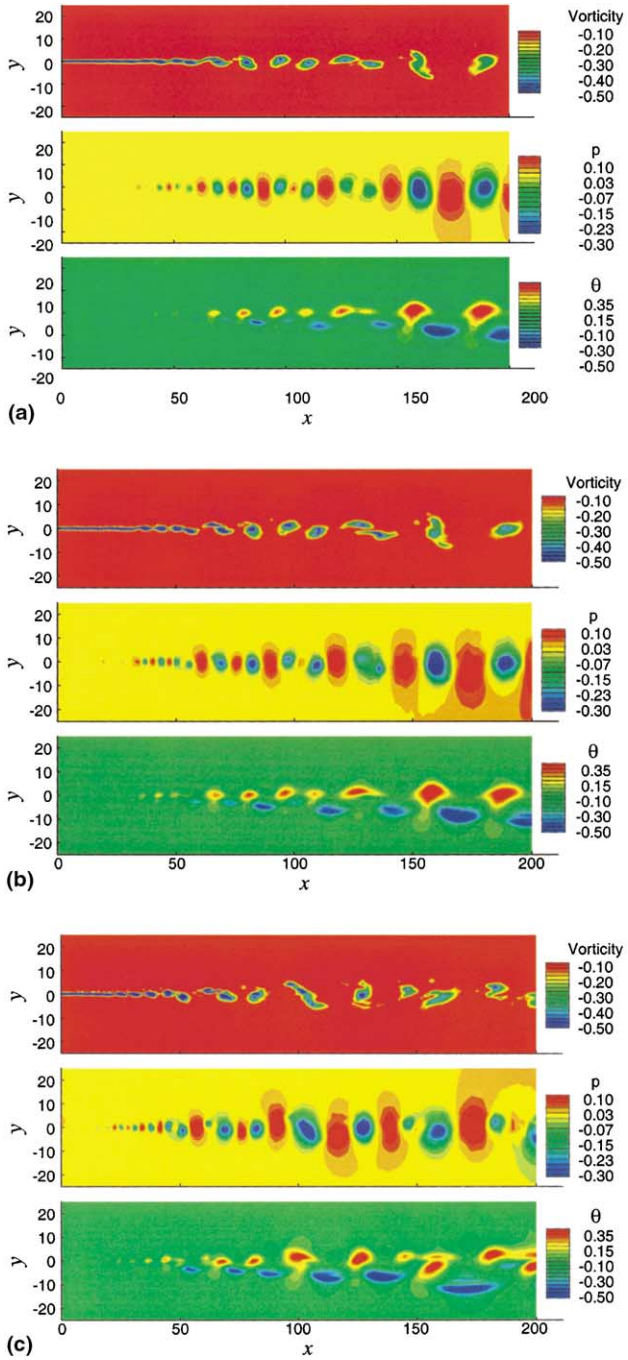

Fig. 5. Instantaneous vorticity, pressure and total temperature distribution when $t = 250$: (a) $Re_{\delta_0} = 200$; (b) $Re_{\delta_0} = 500$; (c) $Re_{\delta_0} = 1000$.

of change and magnitude of $S_{\min}$ are larger than those for $S_{\max}$. It is believed that this difference comes from different pathlines between the upper and lower halves of the shear layer. Further study is required to explain this.

4. Conclusion

A numerical study examines the instantaneous mechanism of energy separation in shear layers with different Re_{δ_0}. Two-dimensional Navier–Stokes equa-

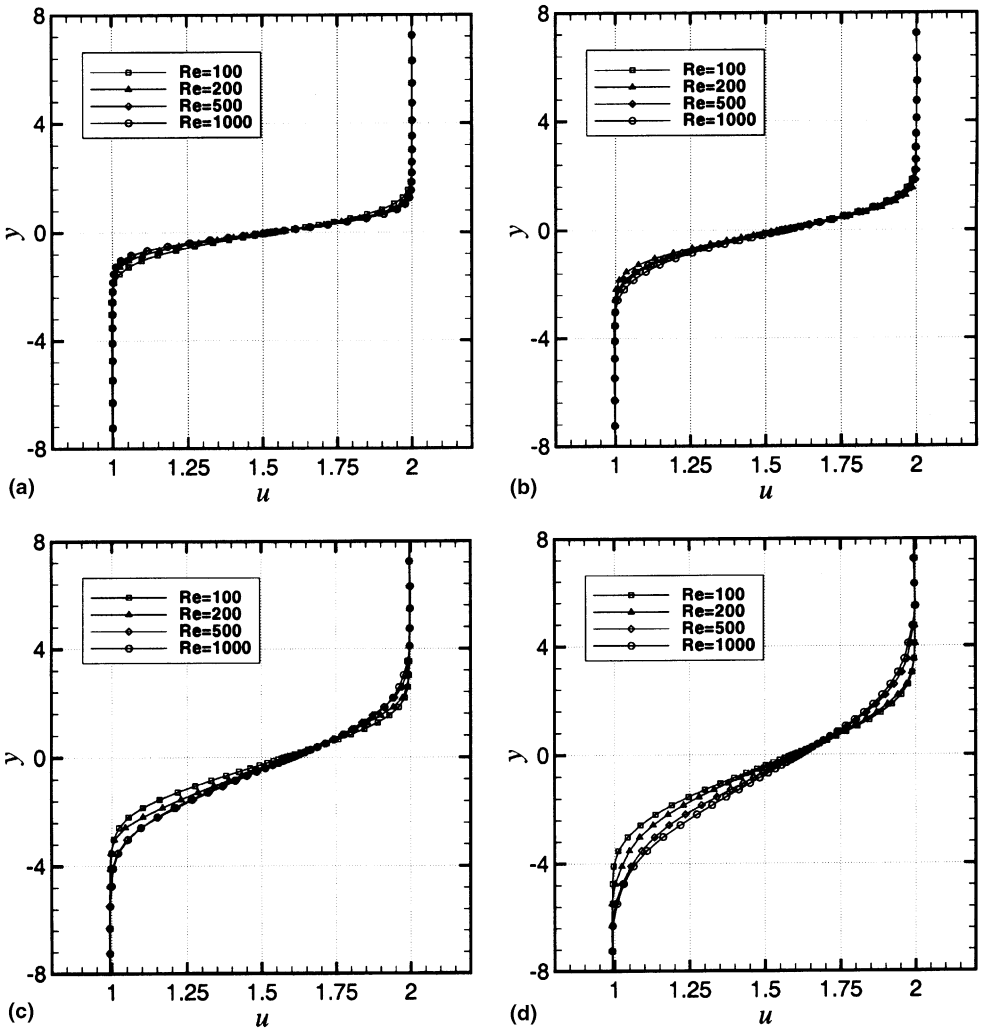

Fig. 6. Time-averaged velocity profile at: (a) $x = 25$; (b) $x = 50$; (c) $x = 75$; (d) $x = 100$.

tions with total energy equation are solved simultaneously. To identify the effect of Re_{δ_0}, shear layers with four different Re_{δ_0} – 100, 200, 500, and 1000 – are simulated. The following conclusions can be obtained from the results.

1. Transport of vortices in the large coherent structure induces pressure fluctuation in flow fields. Fluid which flows through the disturbed pressure field exchanges pressure work with the surrounding fluid, and separates into higher and lower total energy regions.
2. Energy separation due to the pressure fluctuation is a much stronger process than that due to the imbalance between shear work and heat conduction.
3. As Re_{δ_0} increases, the energy separation is intensified due to more rapid development of vortices. Even though random mixing between hot and cold fluids is induced by turbulence for high Re_{δ_0}, energy separation is not significantly lessened over the range of cases studied.

Acknowledgements

This work was supported by the Engineering Research Program of the Office of Basic Energy Sciences at the US Department of Energy. The authors would like to thank Dr. S. Garrick for his comments and discussion on the computational code development. The present study was carried out with IBM SP supercomputer at the University of Minnesota Supercomputing Institute.

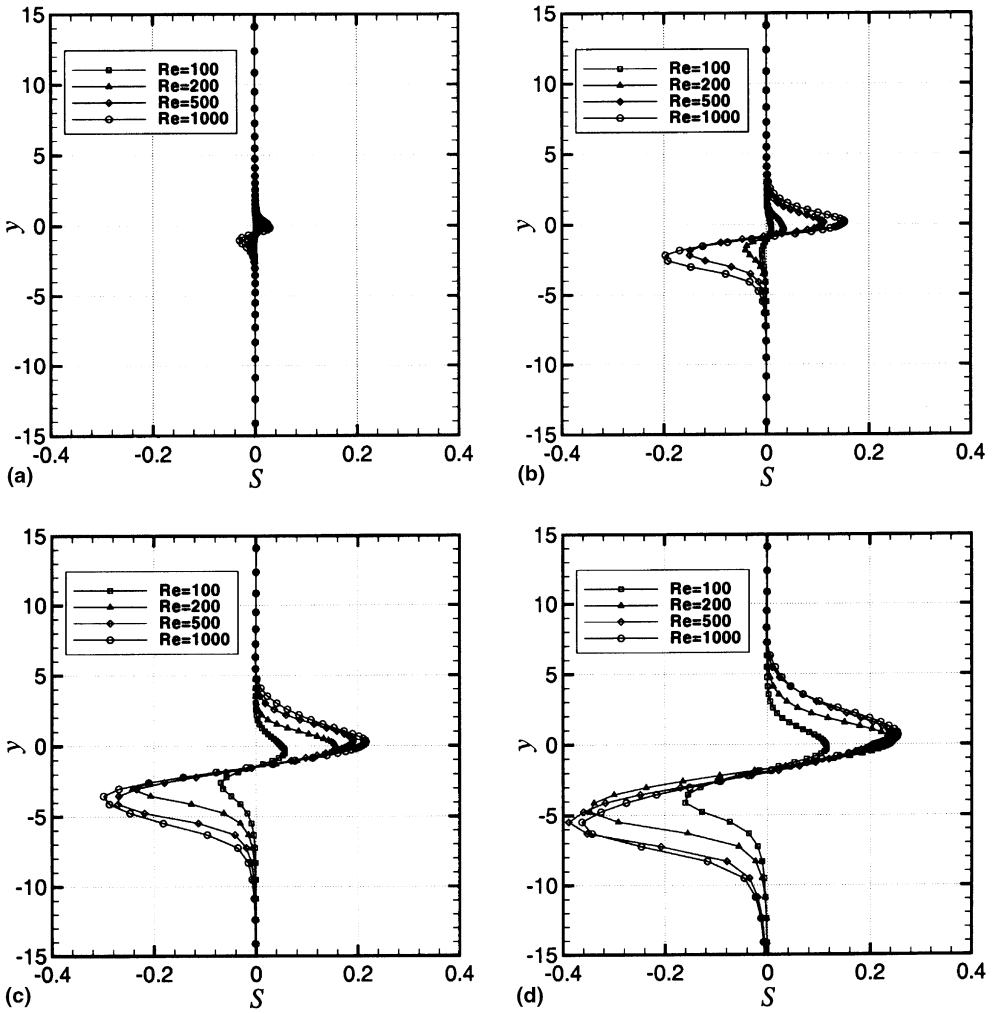

Fig. 7. Time-averaged total temperature profile at: (a) $x = 25$; (b) $x = 50$; (c) $x = 75$; (d) $x = 100$.

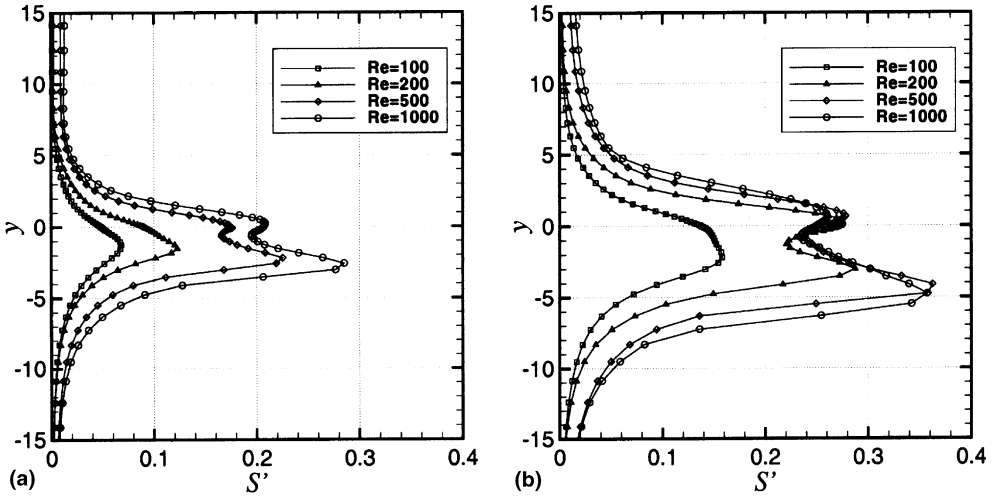

Fig. 8. Total temperature fluctuation profile at: (a) $x = 50$; (b) $x = 75$.

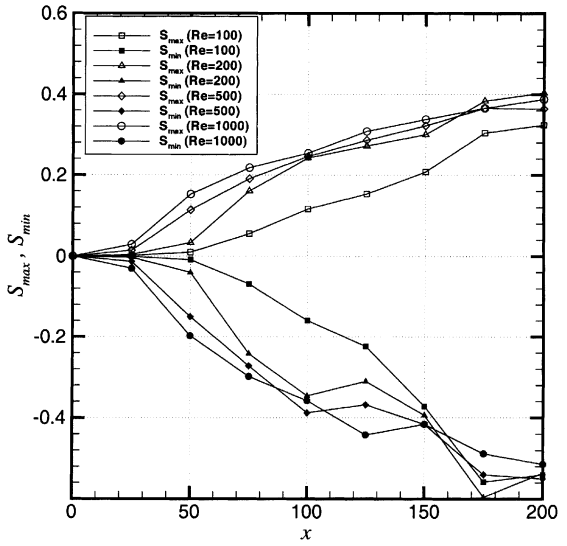

Fig. 9. Streamwise variation of $S_{\max}$ and $S_{\min}$.

References

[1] E. Eckert, W. Weise, Messungen der temperaturverteilumg auf der overfläche schnell angeströmter unberheizter körper, Jahrb deutschen Luftfahrtforsch II (1940) 25–31.

[2] E. Eckert, O. Drewitz, Die berechnung des temperaturefeldes in der laminaren gren-zschichtschnell angeströmter unbeheizter körper, Luftfahrtforschung 19 (1941) 189.

[3] W.S. Seol, R.J. Goldstein, Energy separation in a jet flow, J. Fluid Eng. 119 (1997) 74–82.

[4] M. Kurosaka, J.B. Gertz, J.E. Graham, J.R. Goodman, P. Sundaram, W.C. Riner, H. Kuroda, W.L. Hankey, Energy separation in a vortex street, J. Fluid Mech. 178 (1987) 1–29.

[5] J.J. O'Callaghan, M. Kurosaka, Vortex-induced energy separation in shear flows, AIAA J. 31 (1993) 1157–1159.

[6] E.R.G. Eckert, Cross transport of energy in fluid streams, Wärme-und Stoffübertranung 21 (1987) 73–81.

[7] W.F. Ng, W.M. Chakroun, M. Kurosaka, Time-resolved measurements of total temperature and pressure in the vortex street behind a cylinder, Phys. Fluids A 2 (1990) 971–978.

[8] W.E. Carscallen, T. Currie, S.I. Hogg, J.P. Gostelow, Measurement and computation of energy separation in the vortical wake flow of a turbine nozzle cascade, Technical Report, ASME 98-GT-477, 1998.

[9] M.D. Fox, M. Kurosaka, L. Hedges, K. Hirano, The influence of vortical structure on thermal fields of jets, J. Fluid Mech. 255 (1993) 447–472.

[10] B. Han, R.J. Goldstein, Instantaneous energy separation in shear layer, in: Proceedings of the Seventeenth Symposium on Energy Engineering Science, Argonne National Laboratory, Argonne, IL, 1999, pp. 63–73.

[11] F.M. White, Viscous Fluid Flow, McGraw-Hill, New York, 1991, pp. 500–503.

[12] H.G. Choi, H. Choi, J.Y. Yoo, A fractional four-step finite element formulation of the unsteady incompressible Navier–Stokes equations using supg and linear equal-order element methods, Comput. Methods Appl. Mech. Eng. 143 (1997) 333–348.

[13] N.D. Sandham, W.C. Reynolds, Some inlet-plane effects on the numerical simulated spatially-developing mixing layer, Turbulent Shear Flow 6, Springer, Berlin, 1989, pp. 441–454.

[14] P.M. Gresho, Some current CFD issues relevant to the incompressible Navier–Stokes equations, Comput. Methods Appl. Mech. Eng. 87 (1991) 201–252.

[15] A.K.M.F. Hussain, K.B.M.Q. Zaman, Vortex pairing in a circular jet under controlled excitation Part 2 – coherent structure dynamics, J. Fluid Mech. 101 (1980) 493–544.

[16] A.K.M.F. Hussain, Coherent structures and turbulence, J. Fluid Mech. 173 (1986) 303–356.

[17] C.M. Ho, P. Huerre, Perturbed free shear layers, Ann. Rev. Fluid Mech. 16 (1984) 365–424.